Archival Report

Biological Psychiatry: GOS

White Matter Changes Following Chronic Restraint Stress and Neuromodulation: A Diffusion Magnetic Resonance Imaging Study in Young Male Rats

Bhedita Jaya Seewoo, Kirk Wayne Feindel, Yerim Won, Alexander Clemens Joos, Abbey Figliomeni, Lauren Anne Hennessy, and Jennifer Rodger

ABSTRACT

BACKGROUND: Repetitive transcranial magnetic stimulation (rTMS), a noninvasive neuromodulation technique, is an effective treatment for depression. However, few studies have used diffusion magnetic resonance imaging to investigate the longitudinal effects of rTMS on the abnormal brain white matter (WM) described in depression.

METHODS: In this study, we acquired diffusion magnetic resonance imaging from young adult male Sprague Dawley rats to investigate 1) the longitudinal effects of 10- and 1-Hz low-intensity rTMS (LI-rTMS) in healthy animals; 2) the effect of chronic restraint stress (CRS), an animal model of depression; and 3) the effect of 10 Hz LI-rTMS in CRS animals. Diffusion magnetic resonance imaging data were analyzed using tract-based spatial statistics and fixel-based analysis.

RESULTS: Similar changes in diffusion and kurtosis fractional anisotropy were induced by 10- and 1-Hz stimulation in healthy animals, although changes induced by 10-Hz stimulation were detected earlier than those following 1-Hz stimulation. Additionally, 10-Hz stimulation increased axial and mean kurtosis within the external capsule, suggesting that the two protocols may act via different underlying mechanisms. Brain maturation–related changes in WM, such as increased corpus callosum, fimbria, and external and internal capsule fiber cross-section, were compromised in CRS animals compared with healthy control animals and were rescued by 10-Hz LI-rTMS. Immunohistochemistry revealed increased myelination within the corpus callosum in LI-rTMS–treated CRS animals compared with those that received sham or no stimulation.

CONCLUSIONS: Overall, decreased WM connectivity and integrity in the CRS model corroborate findings in patients experiencing depression with high anxiety, and the observed LI-rTMS–induced effects on WM structure suggest that LI-rTMS might rescue abnormal WM by increasing myelination.

https://doi.org/10.1016/j.bpsgos.2021.08.006

Depression is a heterogeneous disorder affected by subject-related variables, such as sex, age, diet, and genetic background (1), and up to one third of adults are treatment resistant. Repetitive transcranial magnetic stimulation (rTMS) has been used clinically for treatment-resistant depression for over a decade (2), but its underlying mechanisms are still unclear. While translational animal models of depression do not replicate the full complexity of human mood disorders, they can provide homogeneous endophenotypes of depression that facilitate the investigation of causal effects (e.g., genetic and environmental factors) and the efficacy of treatments such as rTMS (3). The chronic restraint stress (CRS) depression model in Sprague Dawley rats has been validated in several pharmacological and magnetic resonance imaging (MRI) studies. Following CRS, animals exhibit changes resembling those found in human depression, including altered behavior (4,5), gene expression (6), and protein levels (7); dysfunctional connectivity (8); reduced glutamate and glutamine levels (5); and hippocampal atrophy (5,9,10).

One of the least understood aspects of depression in patients is related to the microstructural changes often present in the white matter (WM). Diffusion MRI (dMRI) measures the diffusion of water and enables in vivo investigation of tissue microstructure and macro organization of fiber bundles. Water diffusion has been shown to be increased in patients with depression (11,12) and in other animal models of depression (13,14) using several dMRI measures, including mean diffusivity, a global measure of water diffusion, and radial kurtosis, a measure of diffusion restriction perpendicular to axonal direction. These different measures that can be derived from dMRI data are known to provide complementary and partly overlapping information by reflecting changes in WM integrity, specifically with respect to cell density, size, and membrane permeability. Myelin content, known to decrease in depression

SEE COMMENTARY ON PAGE 92

ISSN: 2667-1743 Biological Psychiatry: Global Open Science April 2022; 2:153–166 www.sobp.org/GOS

(15,16), is a key factor that drives the changes in dMRI measures, and this has been demonstrated in mice with demyelination (17,18).

We recently acquired multimodal MRI data following low-intensity rTMS (LI-rTMS) in healthy rats [resting-state functional MRI and magnetic resonance spectroscopy data published in (19)] and following CRS [resting-state functional MRI, magnetic resonance spectroscopy, and hippocampal volume data (5)]. In this study, we analyzed the dMRI data acquired in these experiments to investigate changes in the WM of healthy rats following LI-rTMS and CRS. We also report diffusion changes and myelin changes in the WM in the CRS model following LI-rTMS treatment.

METHODS AND MATERIALS

Animals

Experimental procedures were approved by the University of Western Australia Animal Ethics Committee (RA/3/100/1430 and RA/3/100/1640). Young adult male Sprague Dawley rats (5–8 weeks old, 150–250 g) from the Animal Resources Centre (Canning Vale, Western Australia) were maintained in a temperature-controlled animal care facility on a 12-hour light-dark cycle with food and water ad libitum. The CRS procedure was carried out for 2.5 hours/day for 13 consecutive days as described previously (5). Animals receiving LI-rTMS were habituated to handling and the coil as described previously (20,21). LI-rTMS was delivered using a custom-built round coil (Supplement) at an intensity of approximately 13 mT at the surface of the cortex (22). During the sham procedure, the coil was disconnected.

Healthy animals from Seewoo *et al*. (19) did not undergo the CRS procedure but received 10 minutes LI-rTMS at 10 Hz (n = 9; $CRS^-/10Hz^+$) or 1 Hz (n = 9; $CRS^-/1Hz^+$) to the right brain hemisphere once daily for 15 days (Figure 1A). For the CRS experiments (B.J. Seewoo, B.Sc. Hons, *et al*., unpublished data, July 2020) and data from (5)], animals were randomly assigned to one of the following groups: 1) $CRS^+/10Hz^+$animals (n = 22) underwent CRS and received accelerated 10-Hz LI-rTMS (10 min 3 times daily, 1 hour apart, 5 days/week for 2 weeks) to the left hemisphere; 2) $CRS^+/0Hz^+$ (n = 21) animals underwent CRS and sham LI-rTMS; 3) $CRS^+/0Hz^-$ (n = 19) restraint control animals underwent CRS but did not receive any stimulation; and 4) $CRS^-/0Hz^-$ (n = 8) healthy control animals did not undergo CRS or stimulation (Figure 1B). Because we have previously shown that 1-Hz stimulation has milder effects than 10 Hz (19), only 10-Hz LI-rTMS was used for the next experiments to investigate its effects in more detail in the depression model. Additionally, a pilot study comparing the effects of the accelerated 10-Hz LI-rTMS protocol (3 stimulation sessions/day) and the standard 10-Hz protocol (1 stimulation session/day) showed significant improvement in depression-like behaviors in animals receiving accelerated LI-rTMS only (23). Therefore, only accelerated LI-rTMS was delivered in the CRS experiments.

MRI Data Acquisition

Anesthesia and physiological monitoring were performed as previously described (5). MRI data acquisition time points for the $CRS^-/10Hz^+$ and $CRS^-/1Hz^+$ animals have been previously described (19) (Figure 1A). For the CRS experiments, baseline dMRI data were acquired, followed by the CRS procedure and post-CRS dMRI (Figure 1B). LI-rTMS was then delivered with weekly imaging. MRI data were also acquired 7 and 14 days after stimulation cessation.

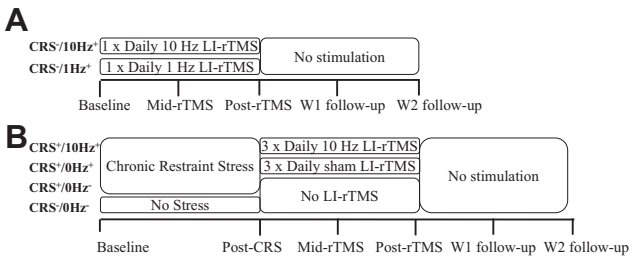

Figure 1. Timeline of an experiment. **(A)** Timeline for the Seewoo *et al.* (19,23) studies, which consisted of 2 weeks of daily 10-minute stimulation at 10 Hz (10 pulses/s, total of 6000 pulses) or 1 Hz (1 pulse/s, total of 600 pulses) delivered to healthy animals. **(B)** Timeline for the CRS model experiments, which consisted of 4 groups of animals. $CRS^+/10Hz^+$, $CRS^+/0Hz^+$, and $CRS^+/0Hz^-$ groups were all subjected to the CRS procedure, but $CRS^+/10Hz^+$ animals received accelerated 10-Hz LI-rTMS (10 pulses/s, total of 6000 pulses delivered 3 times daily, 1 hour apart, 5 days a week for 2 weeks), $CRS^+/0Hz^+$ animals received a sham version of the stimulation protocol, and $CRS^+/10Hz^-$ received no stimulation or extra handling. The $CRS^-/0Hz^-$ animals were not subjected to the CRS procedure and did not receive any stimulation or extra handling. The animals from both **(A)** and **(B)** had 5 sessions of magnetic resonance imaging scans, each separated by at least 1 week, and stimulation (if any) was ceased at the post-rTMS time point. CRS, chronic restraint stress; LI-rTMS, low-intensity repetitive transcranial magnetic stimulation; W1, 1 week after stimulation cessation; W2, 2 weeks after stimulation cessation.

MRI hardware and software setup has been described previously (19) (Supplement). B0 shimming was completed for a region of interest covering the brain using the Bruker Mapshim routine before dMRI data acquisition using a spin-echo echo-planar imaging sequence. Five nondiffusion images were also acquired during each dMRI scan.

$CRS^-/10Hz^+$ and $CRS^-/1Hz^+$ animals were imaged with the following imaging parameters: repetition time = 2800 ms, echo time = 21.0 ms, field of view = 28.2 × 21.0 mm^2, matrix size = 94 × 70, 21 coronal slices (scanner axial), thickness = 1 mm, in-plane resolution = 0.3 × 0.3 mm^2, diffusion duration (δ) = 3.5 ms, and diffusion gradient separation (Δ) = 11 ms. Multishell dMRI data consisted of 30 diffusion gradient directions, b-values = 1000 and 2000 s/mm^2, and imaging time = 6 minutes 4 seconds.

For the CRS experiments, two dMRI datasets were acquired with the following imaging parameters: repetition time = 3000 ms, echo time = 20.8 ms, field of view = 25.6 × 21.6 mm^2, matrix size = 64 × 54, 29 axial slices (scanner coronal), thickness = 0.4 mm, in-plane resolution = 0.4 × 0.4 mm^2, δ = 3.5 ms, and Δ = 12 ms. Single-shell dMRI data consisted of 81 diffusion sampling directions with b-value = 3000 s/mm^2 and imaging time = 8 minutes 36 seconds. Multishell dMRI data consisted of 30 diffusion gradient directions, b-values = 1000 and 2000 s/mm^2, and imaging time = 6 minutes 30 seconds.

dMRI Data Analysis

dMRI data processing was carried out using the MRtrix3 software package (24) and included denoising (25–27), removal of Gibbs ringing artifacts (28), and B1 field inhomogeneity correction (29). Skull stripping was performed using the qimask utility from QUantitative Imaging Tools (30).

Tract-Based Spatial Statistics. Multishell dMRI datasets were analyzed using the tract-based spatial statistics (TBSS) method (31) in the FSL (version 6.0.3) (32) and adapted for using rodent data (Supplement). First, the preprocessed datasets were converted to NifTI file format (https://nifti.nimh.nih.gov/). Diffusion kurtosis parameter maps for fractional anisotropy (FA), mean diffusivity (MD), axial diffusivity (AD), radial diffusivity (RD), kurtosis fractional anisotropy, mean kurtosis, mean kurtosis tensor, axial kurtosis (AK), and radial kurtosis (RK), as well as diffusion tensor parameter maps for FA, MD, AD, and RD, were then generated for each animal at each time point using the diffusional kurtosis estimator (33). Next, the SPM12 toolbox (using MATLAB, version 9.10.0.1602886 (R2021a) [The MathWorks, Inc.] compiler) was used to convert the above parameter maps into a format compatible with input through the DTI-ToolKit software. DTI-ToolKit was then used to spatially normalize each dataset to a population-specific template (34) using a tensor-based registration formulation (35). These coregistered images were concatenated to create one single 4-dimensional image for each diffusion parameter and fed into the FSL/TBSS pipeline.

The mean of all FA images was computed and used to generate a mean FA skeleton and a skeleton mask using an FA threshold of 0.26 (36). The mean FA and mean FA skeleton mask were used to skeletonize all parameter maps, which were then fed into the voxelwise analysis using nonparametric permutation testing (FSL/randomise).

Fixel-Based Analysis. Single-shell dMRI data were used to generate and analyze fixel-based metrics, including the apparent fiber density (AFD), fiber cross-section (FC), and the combination of AFD and FC (FDC), using the multitissue fixel-based analysis pipeline implemented in MRtrix3 as outlined previously (37–40). In this study, a population-based template was generated based on 50 datasets across groups and time points. Whole-brain tractography was performed on the template with probabilistic tracking at a cutoff of 0.2 (41).

For track-weighted imaging analysis, whole-brain tractography was performed in native space for each rat using the same parameters outlined above and registered to the study-specific template to normalize both the length and spatial location of the streamlines. The normalized tractograms were then used to generate the average pathlength map (APM), representing the average length of tracks passing through each voxel (42), and mean curvature map, representing the average curvature of all tracks passing through each voxel.

Differences between time points were determined using nonparametric permutation testing over 5000 permutations (43,44).

Statistical Analyses. Because of the longitudinal nature of the data presented, within-group comparisons were performed to investigate changes over time. To quantify the amount of change with and without restraint, baseline and postrestraint time points were compared using an equal number of animals from the $CRS^{-}/0Hz^{-}$ and $CRS^{+}/0Hz^{-}$ groups (n = 8). For all image analyses, all voxels in the brain were corrected using the threshold-free cluster enhancement method with familywise error correction (45). Statistically significant differences for maps were visualized at a Bonferroni-corrected p value of .006 (rTMS effects) and .025 (CRS effects). In addition, raw diffusion values from 4 regions of interest (ROIs) within the corpus callosum, internal capsule, external capsule, and fimbria [manually drawn using ITK-SNAP 3.3.0 (46); http://www.itksnap.org] were extracted and analyzed using RStudio (version 3.6.1; RStudio Team). Analysis of variance (lmerTest package) was utilized to test for any significant effect of animal group or time point. When there was an effect of both animal group and time point, post hoc pairwise comparisons were performed with false discovery rate correction (emmeans package) to determine significant differences in diffusion parameters between time points for each group and ROI.

Brain Immunohistochemistry

At the end of the study, the rats were euthanized with an overdose of sodium pentobarbitone (>160 mg/kg intraperitoneal) and transcardially perfused with 200 mL of 4% paraformaldehyde in 0.2M phosphate buffer. Brains were postfixed in 4% paraformaldehyde solution at 4 °C and transferred to 30% sucrose in phosphate-buffered saline 48 hours before cryosectioning into 40-μm coronal sections. Five brains from each of the $CRS^{+}/10Hz^{+}$, $CRS^{+}/0Hz^{+}$, and $CRS^{+}/0Hz^{-}$ groups were selected and 3 sections were chosen per brain for immunohistochemical staining at positions 80, 88, and 97 on our MRI population template corresponding to bregma −3.11, −2.11, and −0.11 mm (47). Sections were processed for immunohistochemistry (Supplement) using rabbit anti-myelin basic protein polyclonal antibody (ab40390) and anti-NeuN monoclonal antibody (MAB377). Sections were imaged on a Nikon confocal C2, NI-E microscope with a 10× lens, captured using NIS Elements AR software using the same settings and analyzed using FIJI (ImageJ 1.53c, National Institutes of Health) software by an operator blinded to conditions (48) (Supplement). Data were analyzed and plotted using RStudio (version 3.6.1; RStudio Team). Analysis of variance (lmerTest package) was utilized to test for any significant effect of animal group or ROI. Post hoc Mann-Whitney two-sample rank-sum test with false discovery rate correction (rstatix package) was then used to determine significant differences in myelin basic protein (MBP) intensity between groups.

RESULTS

WM Changes Following 10- and 1-Hz LI-rTMS in Healthy Rats

We first examined whether LI-rTMS-induced any changes in WM tracts in healthy rats. TBSS analysis of the 10- and 1-Hz data revealed an increase in diffusion kurtosis imaging/diffusion tensor imaging (DKI/DTI) FA for both frequencies. This increase was detectable at the 7 days after stimulation cessation time point in the 10-Hz group but was observed only

at the 14 days after stimulation cessation time point in the 1-Hz group (Figure 2). In addition, only the 10-Hz group exhibited an increase in external capsule AK, internal and external capsule kurtosis FA and mean kurtosis, and fimbria and external capsule mean kurtosis tensor (Figures 2 and 3). ROI-based analyses showed that both groups showed an increase in internal capsule DTI/DKI FA, but only the 1-Hz group showed an increase in fimbria DTI FA (Figure 3). Additionally, internal capsule AD and fimbria RK increased in the 10-Hz group only and corpus callosum RK increased in both groups (Figure S1).

Rat Model of Depression: WM Changes Following CRS

Having demonstrated that LI-rTMS altered WM tracts in healthy animals, it was relevant to examine the effects of LI-rTMS in a disease model. rTMS is an FDA-approved treatment of depression, and therefore a rat model of depression (CRS) was chosen. We first report CRS-induced WM changes in restrained animals compared with healthy unrestrained animals.

Changes in WM diffusion and kurtosis were observed in both restrained and unrestrained groups, likely reflecting brain maturation. DTI AD, DTI/DKI RD, and DTI/DKI MD decreased significantly from baseline at the postrestraint time point, while DKI AD decreased in healthy animals only and AK and DTI FA increased in restrained animals only (Figure 4A). ROI-based analyses showed that both groups exhibited a significant decrease in external capsule DTI RD and increase in external capsule DTI FA, while internal capsule DTI FA increased in restrained animals only and fimbria RK increased in healthy animals only (Figure 5A).

Following restraint, animals exhibited smaller and delayed brain maturation–related changes in WM FC and morphology compared with unrestrained animals. Unrestrained animals showed a greater increase in internal capsule FC and FDC and corpus callosum and fimbria FDC compared with restrained animals (Figure 4B). Additionally, there was a significant increase in AFD, APM, and mean curvature map in unrestrained animals only. ROI-based analyses showed a significant increase in internal capsule FC and corpus callosum and fimbria FDC in both groups. Only the unrestrained animals exhibited a significant increase in corpus callosum, fimbria and external capsule FC, internal capsule FDC, and external capsule and fimbria APM (Figure 5B).

Rat Model of Depression and Treatment: WM Changes Following CRS and Accelerated 10-Hz LI-rTMS

Diffusion MRI. Having identified changes in WM that were induced by CRS, we then determined whether these changes could be rescued using LI-rTMS. Similar to changes reported following CRS, there was a significant increase in DTI FA and FC when comparing postrestraint and 14 days after stimulation cessation time points in all groups (Figure 6), suggesting ongoing brain maturation. LI-rTMS and control groups showed similar amount of change in DTI/DKI FA overall, but only the control group showed changes within the corpus callosum (Figure 7). DKI/DTI RD decreased over time in the corpus callosum in the sham and control groups but decreased over time in the fimbria in the LI-rTMS group (Figure 7). While FC increased with time in all groups, there was a greater increase in FC in the internal capsule and fimbria of the LI-rTMS group compared with sham and control groups, suggesting a

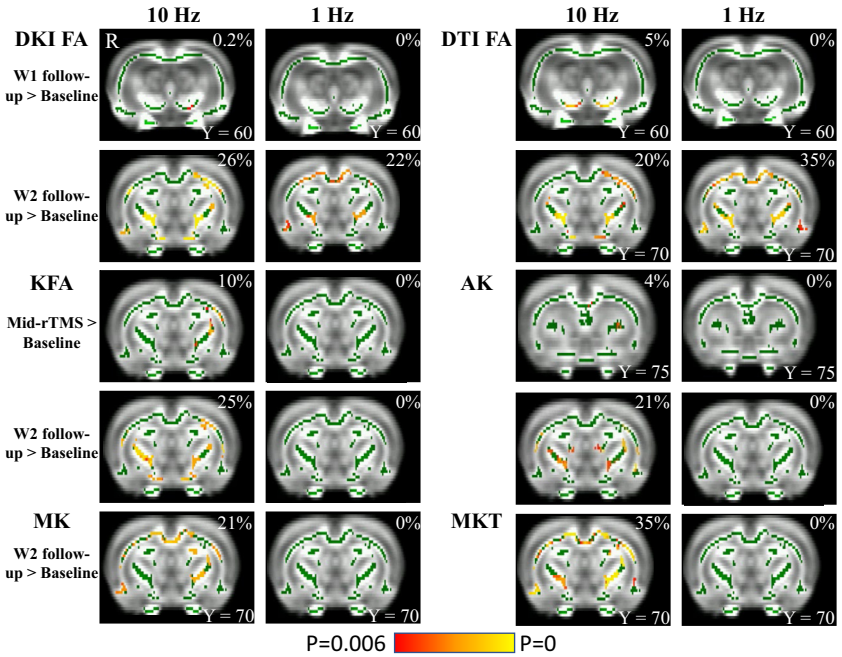

Figure 2. Tract-based spatial statistics analysis shows significant changes in diffusion and kurtosis parameters following 10- or 1-Hz low-intensity rTMS in healthy rats ($p_{Bonferroni} < .006$). The figure illustrates changes between baseline and 4 time points: after 1 (mid-rTMS) and 2 weeks (post-rTMS) of daily stimulation and W1 and W2 follow-up. Green represents mean FA skeleton of all animals; red denotes an increase after stimulation. The percentage in the top-right corner of the coronal slices represents the percentage of the significant voxels relative to the whole skeleton voxels for each parameter. Low-intensity-rTMS was delivered to the right side of the brain (denoted by R). AK, axial kurtosis; DKI, diffusion kurtosis imaging; DTI, diffusion tensor imaging; FA, fractional anisotropy; KFA, kurtosis fractional anisotropy; MK, mean kurtosis; MKT, mean kurtosis tensor; rTMS, repetitive transcranial magnetic stimulation; W1, 1 week after stimulation cessation; W2, 2 weeks after stimulation cessation.

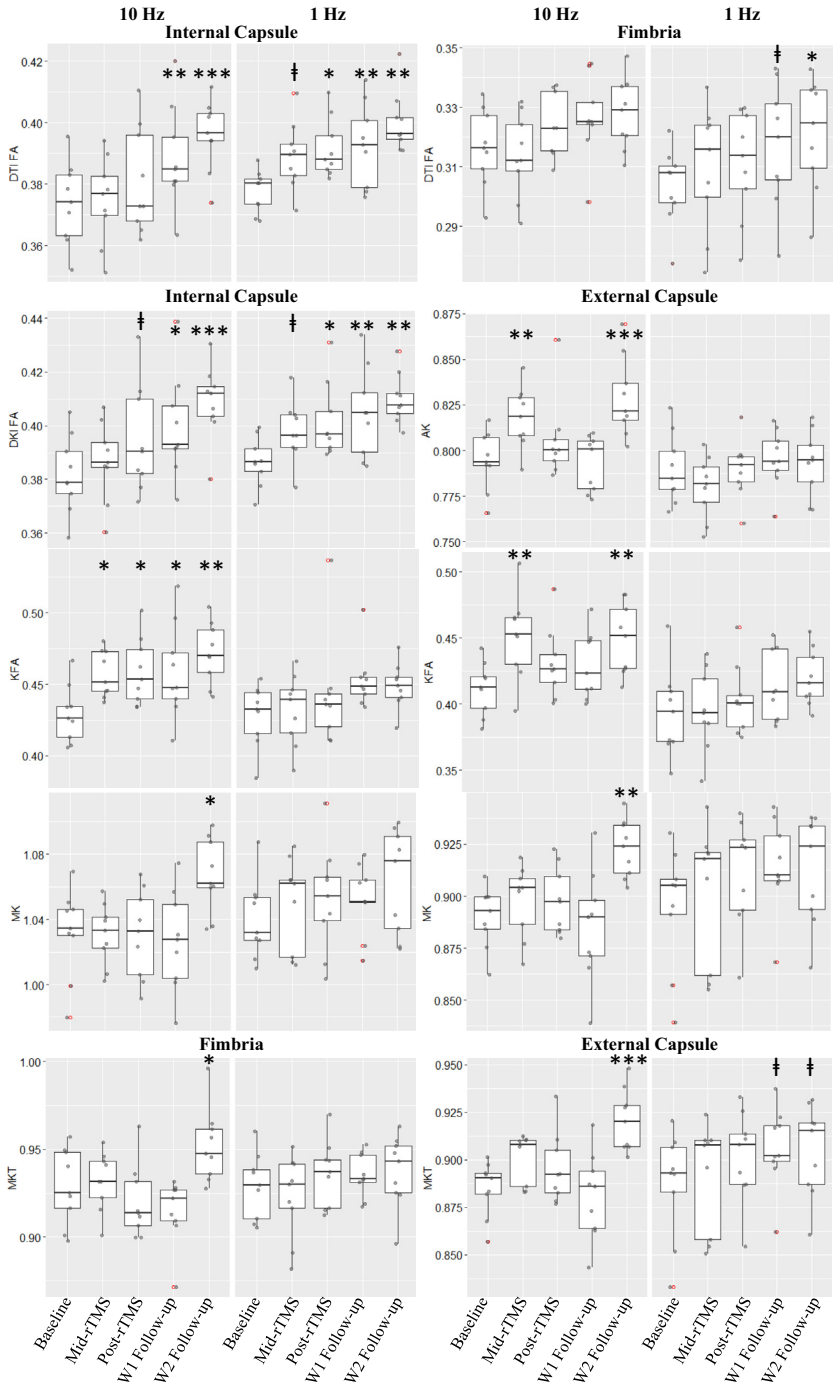

Figure 3. Significant changes in DTI and DKI measures within the internal and external capsules and fimbria in healthy animals receiving 10- or 1-Hz low-intensity rTMS ($p_{FDR} < .006$). The boxplots illustrate changes between baseline and 4 time points: after 1 week (mid-rTMS) and 2 weeks (post-rTMS) of daily stimulation and W1 and W2 follow-up. ‡$p_{FDR} < .1$, *$p_{FDR} < .05$, **$p_{FDR} < .01$, ***$p_{FDR} < .001$. AK, axial kurtosis; DKI, diffusion kurtosis imaging; DTI, diffusion tensor imaging; FA, fractional anisotropy; KFA, kurtosis fractional anisotropy; MK, mean kurtosis; MKT, mean kurtosis tensor; p_{FDR}, false discovery rate-corrected p; rTMS, repetitive transcranial magnetic stimulation; W1, 1 week after stimulation cessation; W2, 2 weeks after stimulation cessation.

significant effect of LI-rTMS in normalizing the WM changes observed postrestraint (Figure 6B). ROI-based analyses showed similar changes in FC and FDC in all groups (Figure S2).

Immunohistochemistry. Given that we found a decrease in DTI and DKI RD after rTMS and that changes in RD are related to myelination, we measured the relative immunodensity of the MBP fluorescent signal in the left, center, and right regions of the corpus callosum in the $CRS^+/10Hz^+$, $CRS^+/0Hz^+$, and $CRS^+/0Hz^-$ groups (Figure 8A). A near-significant difference was detected between groups (analysis of variance, $F_{2,12} = 3.710$; $p = .056$). Given the small sample size (n = 5/group), a post hoc Mann-Whitney two-sample rank-sum test

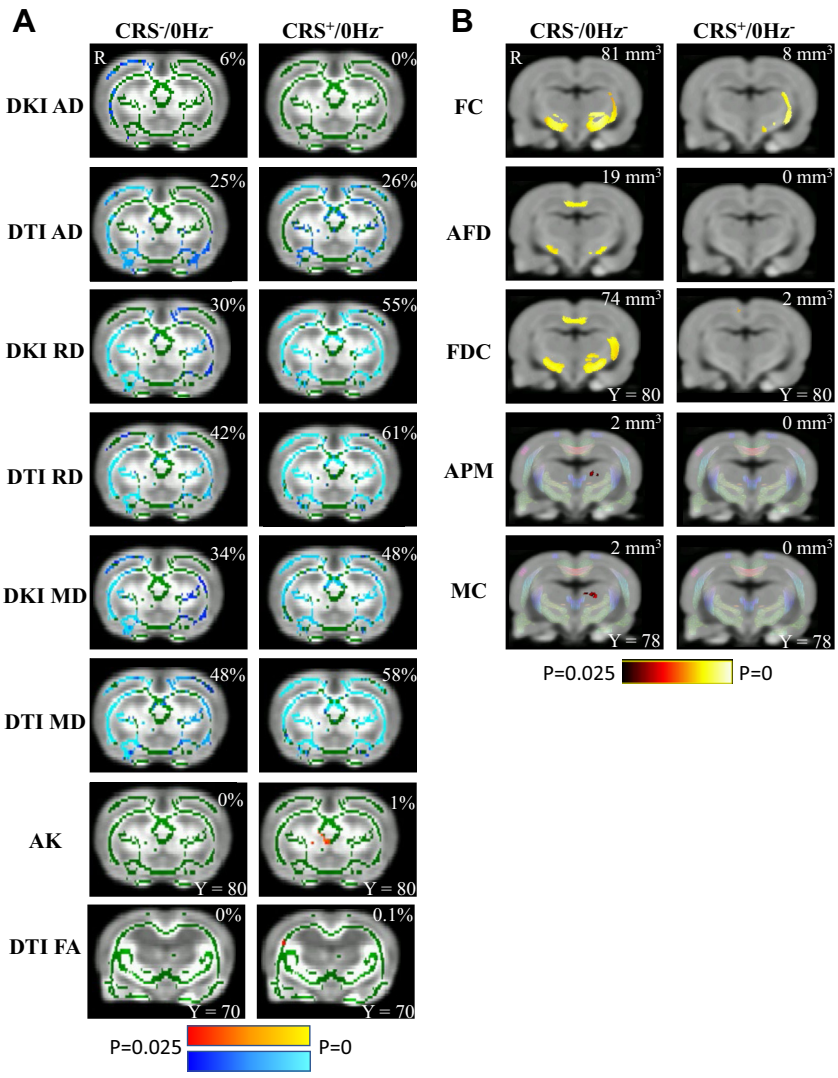

Figure 4. CRS results in significant changes in the white matter ($p_{Bonferroni} < .025$). **(A)** Results from tract-based spatial statistics analysis. Green represents the mean FA skeleton of all animals; red denotes an increase and blue represents a reduction after restraint. The percentage on the top-right corner of each coronal slice represents the percentage of the significant voxels relative to the whole skeleton voxels for each parameter. **(B)** Results from fixel-based analysis and track-weighted imaging. Rats that underwent CRS ($CRS^{+}/0Hz^{-}$) had a smaller increase in FC, AFD, FDC, APM, and MC. Statistically significant fixels are overlaid on the population template. The whole-brain template tractogram is also overlaid on the population template for APM and MC. The number at the top-right corner of each coronal slice represents the volume of significant voxels. The right side of the brain is denoted by R. AD, axial diffusivity; AFD, apparent fiber density; AK, axial kurtosis; APM, average pathlength mapping; CRS, chronic restraint stress; DKI, diffusion kurtosis imaging; DTI, diffusion tensor imaging; FA, fractional anisotropy; FC, fiber cross-section; FDC, combination of AFD and FC; MC, mean curvature; MD, mean diffusivity; RD, radial diffusivity.

was performed. $CRS^{+}/10Hz^{+}$ animals showed greater MBP immunodensity than $CRS^{+}/0Hz^{+}$ animals or $CRS^{+}/0Hz^{-}$ animals at each ROI (Figure 8B). This difference was greater in the left hemisphere, which received LI-rTMS (Table 1), supporting the fixel-based analysis findings that LI-rTMS rescued the delayed myelination caused by CRS.

DISCUSSION

To our knowledge, this study is the first to employ dMRI to track whole-brain WM changes in healthy and CRS animals over time and following multiple sessions of LI-rTMS. While caution is needed when linking diffusion measures to microstructural correlates, based on the current literature, our dMRI and histological findings suggest that the restorative effects of LI-rTMS on WM are at least in part due to an increase in myelination.

High-Frequency LI-rTMS Induces Greater and Faster Changes in the WM of Healthy Rats Than Low-Frequency LI-rTMS

In this study, we observed extensive WM changes in healthy Sprague Dawley rats following 10- and 1-Hz LI-rTMS using both DKI and conventional DTI. The increase in anisotropy observed following 10-Hz stimulation likely stems from the increased axial (parallel) diffusivity observed within the internal capsule, which in turn may result from an increase in packing density of fiber bundles and axons, axonal diameter increase, changes in neurofibrils, and/or increased complexity of extracellular matrix (49). Increased diffusion restriction perpendicular to axonal direction (RK) in the corpus callosum of both groups likely reflects increased myelination and/or number of axons (49). RK is thought to be more influenced by cellular membranes and myelin sheaths, whereas AK (parallel to axonal direction) is considered to be primarily affected by

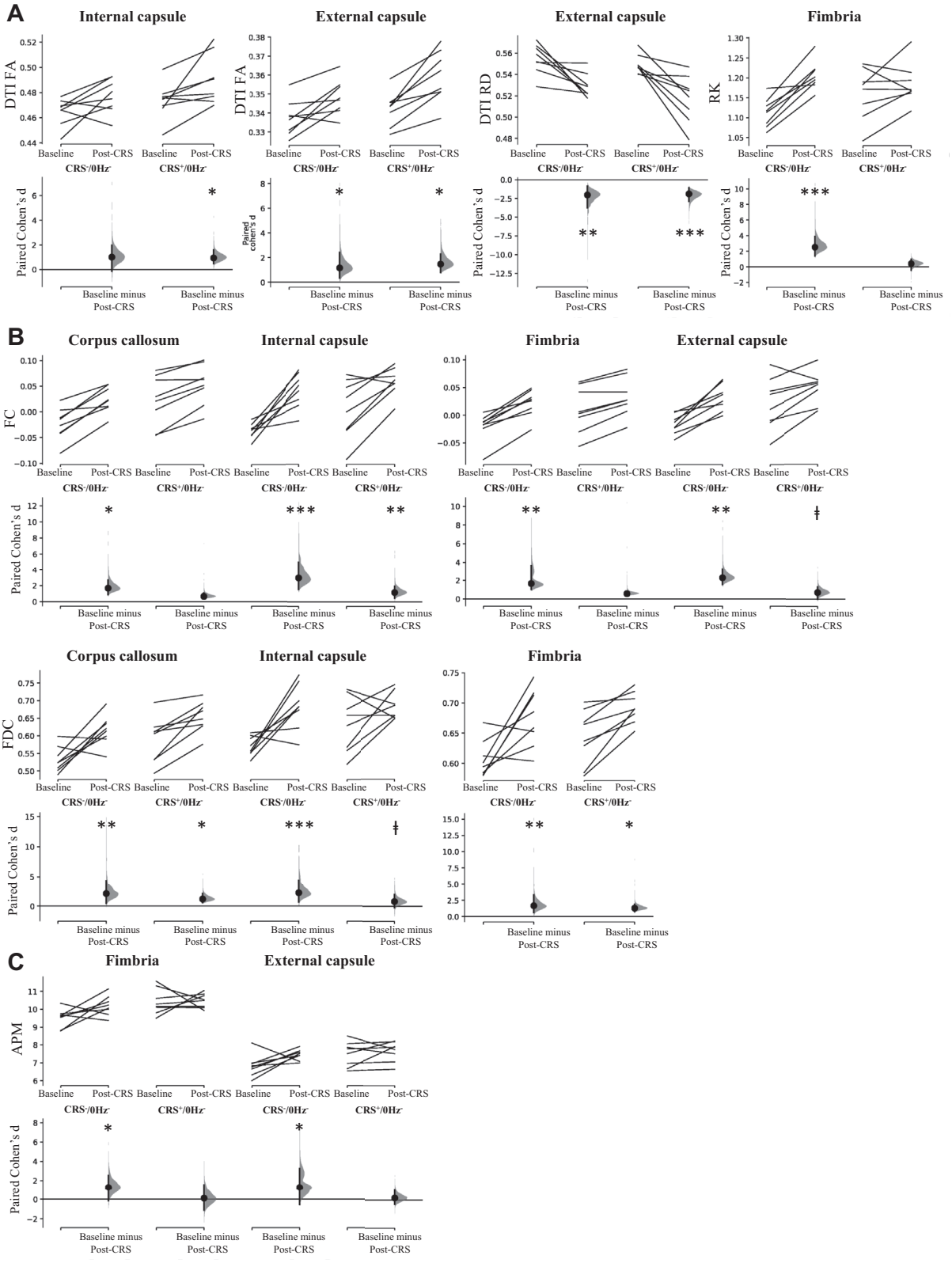
A
Internal capsule
External capsule
External capsule
Fimbria
DTI FA
DTI FA
DTI RD
RK
Baseline
Post-CRS
CRS-/0Hz-
CRS+/0Hz-
Paired Cohen's d
Baseline minus Post-CRS
B
Corpus callosum
Internal capsule
Fimbria
External capsule
FC
FDC
C
Fimbria
External capsule
APM

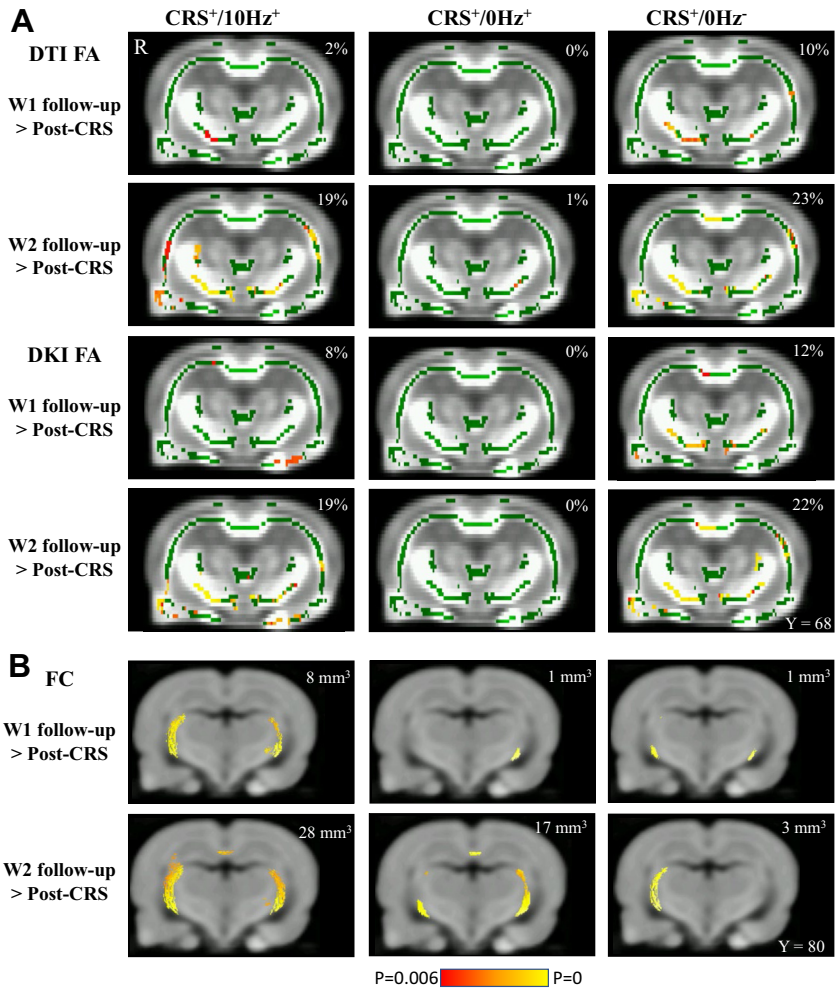

Figure 6. Increase in **(A)** DTI/DKI FA and **(B)** FC following restraint in animals receiving active ($CRS^+/10Hz^+$), sham ($CRS^+/0Hz^+$), and no stimulation ($CRS^+/0Hz^-$). **(A)** Results from tract-based spatial statistics analysis. Green represents the mean FA skeleton of all animals; red denotes an increase after restraint. The percentage on the top-right corner of each coronal slice represents the percentage of the significant voxels relative to the whole skeleton voxels for each parameter. **(B)** Results from the fixel-based analysis. Statistically significant fixels are overlaid on the population template. The number at the top-right corner of each coronal slice represents the volume of significant voxels. The right side of the brain is denoted by R. Low-intensity repetitive transcranial magnetic stimulation was delivered to the left side of the brain. All voxels were thresholded at a minimum Bonferroni-corrected *p* value of .006. CRS, chronic restraint stress; DKI, diffusion kurtosis imaging; DTI, diffusion tensor imaging; FA, fractional anisotropy; FC, fiber cross-section; W1, 1 week after stimulation cessation; W2, 2 weeks after stimulation cessation.

intracellular structures. Although interpreting DKI metrics in terms of tissue microstructure is challenging, a significantly higher AK in the 10 Hz could be considered consistent with higher neurite density and increased microstructural complexity along the axial direction of WM fibers. It will be interesting to determine whether the frequency-specific changes in WM observed here are linked to the frequency-specific effects that have been reported on neuronal excitability, functional connectivity, and neurometabolite changes, among others (50–53).

There are a few dMRI reports on the effect of rTMS on water diffusion in healthy subjects, but only the effects of a single rTMS session were assessed and results were inconclusive. One study reported no changes following high- or low-frequency rTMS (54), in contrast with other 1-Hz stimulation studies finding a brief (5 min) restriction in diffusion within the stimulated region compared with the contralateral region (55), and changes lasting up to 20 minutes were also reported in remote nonstimulated regions (56). One explanation for the longer-lasting effects observed in this study is that 2 weeks of daily repeated rTMS reinforced the changes in diffusion, inducing a long-lasting (cumulative) effect on WM organization and structural integrity within the whole brain (57).

Compromised Brain Maturation–Related Changes Following CRS

Local fiber density, FC, average pathlength, and mean curvature increased from baseline in healthy control animals, which may suggest changes in fiber morphology, an overall

Figure 5. CRS results in significant changes in **(A)** DTI measures and **(B)** FC, FDC, and **(C)** APM within white matter regions. The Cohen's *d* for two comparisons are shown in the Cumming estimation plots. The raw data are plotted on the upper axes; each paired set of observations is connected by a line. On the lower axes, each paired mean difference is plotted as a bootstrap sampling distribution. Mean differences are depicted as dots; 95% confidence intervals are indicated by the ends of the vertical error bars. ‡$p_{FDR} < .1$, *$p_{FDR} < .05$, **$p_{FDR} < .01$, ***$p_{FDR} < .001$. APM, average pathlength mapping; CRS, chronic restraint stress; DKI, diffusion kurtosis imaging; DTI, diffusion tensor imaging; FA, fractional anisotropy; FC, fiber cross-section; FDC, combination of apparent fiber density and FC; p_{FDR}, false discovery rate–corrected *p*; RD, radial diffusivity; RK, radial kurtosis.

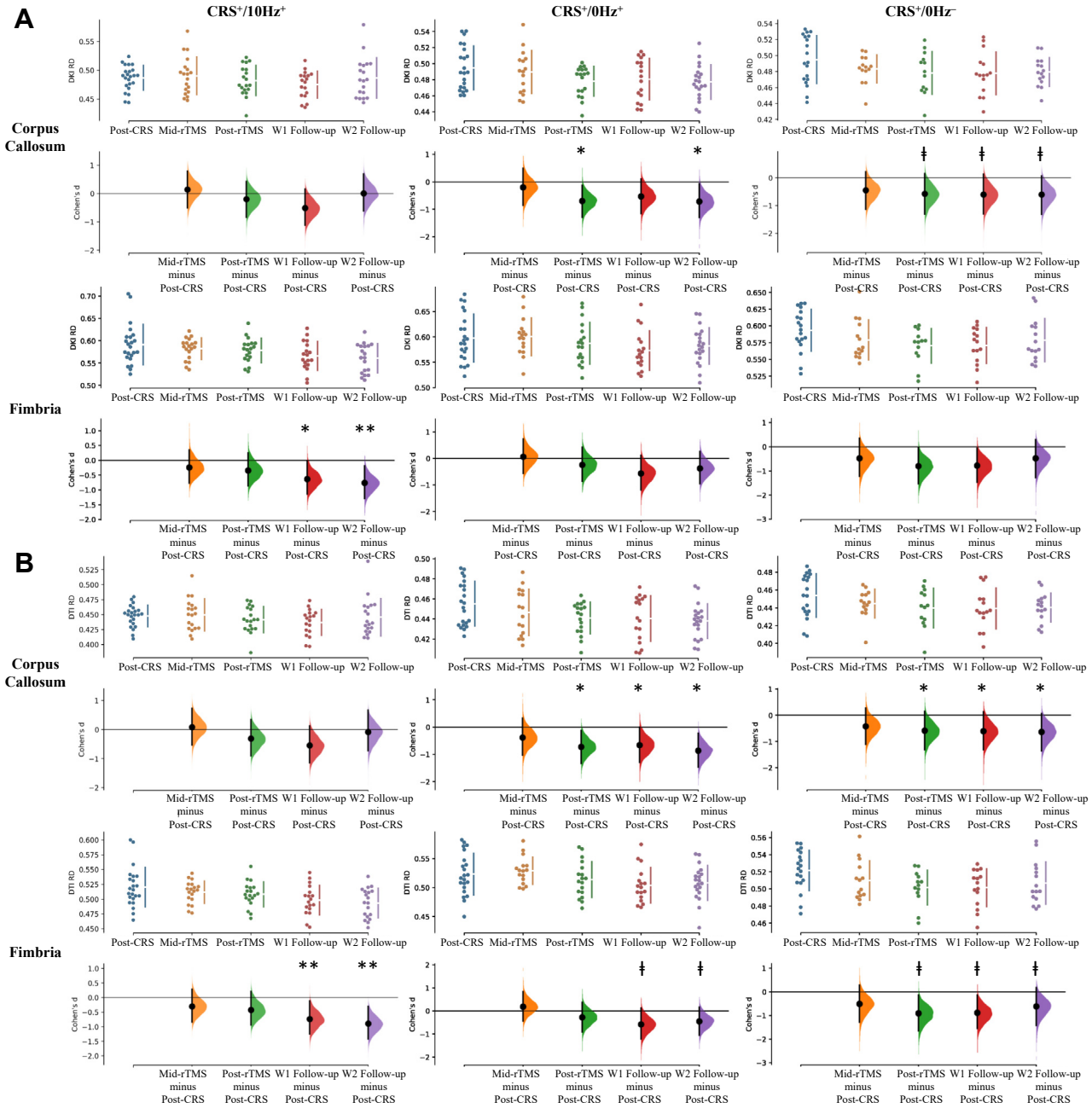

Figure 7. Significant changes in **(A)** DKI RD and **(B)** DTI RD within the corpus callosum and fimbria in animals receiving active (CRS$^+$/10Hz$^+$), sham (CRS$^+$/0Hz$^+$), and no stimulation (CRS$^+$/0Hz$^-$). The Cohen's *d* for four comparisons against the shared control after CRS are shown in the Cumming estimation plot. The raw data are plotted on the upper axes. On the lower axes, mean differences are plotted as bootstrap sampling distributions. Each mean difference is depicted as a dot. Each 95% confidence interval is indicated by the ends of the vertical error bars. ‡$p_{FDR} < .1$, *$p_{FDR} < .05$, **$p_{FDR} < .01$. CRS, chronic restraint stress; DKI, diffusion kurtosis imaging; DTI, diffusion tensor imaging; p_{FDR}, false discovery rate-corrected *p*; RD, radial diffusivity; rTMS, repetitive transcranial magnetic stimulation; W1, 1 week after stimulation cessation; W2, 2 weeks after stimulation cessation.

increase in number of axons, and/or total intra-axonal volume within fiber bundles within the corpus callosum, fimbria, and internal and external capsules (40). These results concur with the work of Mengler *et al.* (58), who reported progressive increases in cortical thickness and volume of several brain regions in healthy rats up until 2 months of age. Moreover, similar to this study, they found a decrease in AD, RD, and MD during the first 6 months of cerebral development (58). Our DTI/DKI measures confirm these findings and further show an increase in fimbria RK, which likely reflects

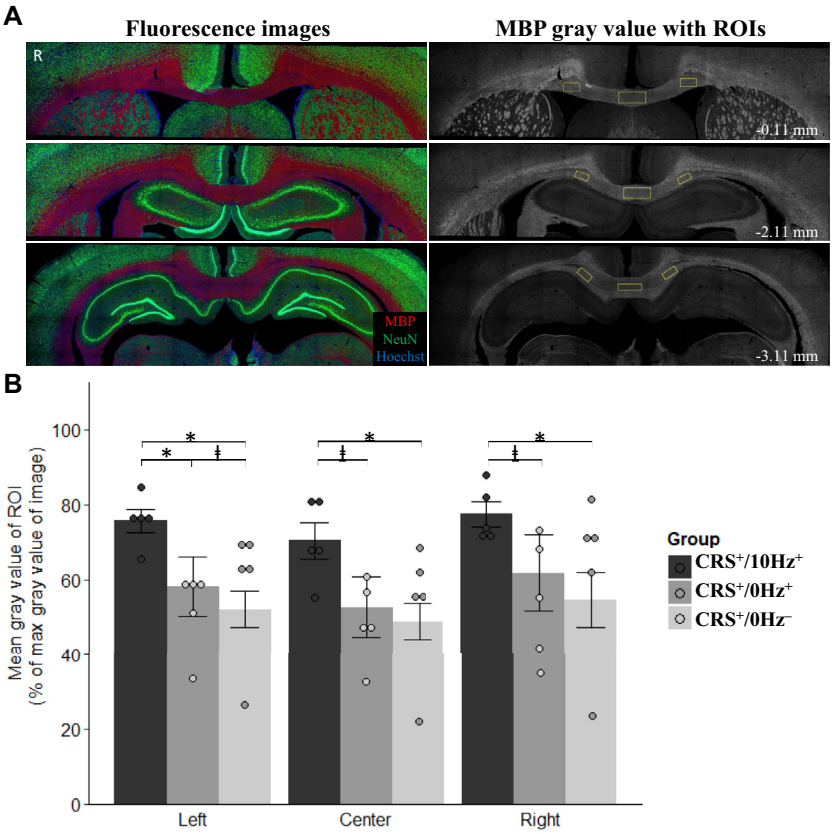

Figure 8. MBP immunostaining in CRS animals receiving active ($CRS^+/10Hz^+$), sham ($CRS^+/0Hz^+$), and no stimulation ($CRS^+/0Hz^-$). **(A)** Representative images of the three sections selected from each brain for immunostaining. Left: original fluorescent signal of MBP staining (red), NeuN (green), and Hoechst signal (blue). Right: gray-scale images of MBP fluorescent signal (white) with left, center, and right ROIs overlaid (yellow) from which immunodensity was measured. Low-intensity repetitive transcranial magnetic stimulation was delivered to the left side of the brain. R represents the right side of the brain. **(B)** Mean ± SEM of the mean gray value of the left, center, and right ROIs measured as the percentage of the maximum gray value of the image. Comparisons were made by Mann-Whitney two-sample rank-sum test with false discovery rate correction. Low-intensity repetitive transcranial magnetic stimulation was delivered to the left side of the brain. ‡$p < .1$, *$p < .05$. CRS, chronic restraint stress; MBP, myelin basic protein; ROI, region of interest.

increased myelination leading to more diffusion restriction radially (49). Overall, our results confirm and extend previous studies of ongoing brain maturation–related changes in young adult rats.

Animals subjected to restraint stress exhibited less of these brain maturation–related changes, with the greatest impact on changes related to fiber morphology (AFD, APM, and mean curvature map). However, the DTI and DKI results are less clear-cut. Microstructural disruption in WM, axonal degeneration, and demyelination in depression are generally believed to produce higher RD and MD and lower FA in both patients with depression (11,59–61) and animal models of depression (62,63), such as the Wistar–Kyoto strain genetic model (14) and chronic unpredicted mild stress model (13). Keeping in mind that relating DTI and DKI measures to tissue microstructure is difficult, our observation of higher FA values being driven by a decrease in RD and MD contradicts the above-mentioned studies. Nevertheless, the heterogeneity of symptoms of depression may lead to these differential microstructural alterations [human: (64–66), animal: (67)]. For example, increased FA and decreased RD can be associated with high levels of anxiety in human depression (65,68,69). Similarly, different animal model strains are prone to variation in behavioral and physiological adaptations to repeated stress and therefore exhibit different changes in dMRI (70). Overall, while the exact pathological processes occurring in patients with depression and CRS animals are still unknown, increased AK and decreased MD and RD strongly suggest that water diffusion is more restricted and WM structure is altered by CRS.

Table 1. Statistical Table Indicating the Results of Immunohistochemistry Data

ROI	$CRS^+/10Hz^+$	$CRS^+/0Hz^+$	$CRS^+/0Hz^-$	$CRS^+/10Hz^+ > CRS^+/0Hz^+$	$CRS^+/10Hz^+ > CRS^+/0Hz^-$	$CRS^+/0Hz^+ > CRS^+/0Hz^-$
Left	76 ± 3	58 ± 8	52 ± 5	$p_{FDR} = .024^a$; ES = .694	$p_{FDR} = .012^a$; ES = .826	$p_{FDR} = .075^b$; ES = .495
Center	70 ± 5	53 ± 8	49 ± 5	$p_{FDR} = .071^b$; ES = .561	$p_{FDR} = .048^a$; ES = .694	$p_{FDR} = .21$; ES = .297
Right	77 ± 3	62 ± 10	55 ± 7	$p_{FDR} = .071^b$; ES = .561	$p_{FDR} = .024^a$; ES = .760	$p_{FDR} = .274$; ES = .231

Values are presented as mean ± SE for each group.
CRS, chronic restraint stress; ES, effect size; p_{FDR}, false discovery rate–corrected p; ROI, region of interest.
[a] $p_{FDR} < .05$
[b] $p_{FDR} < .1$

Accelerated 10-Hz LI-rTMS Rescued Brain Maturation–Related Changes

Given that we have shown changes in WM linked to ongoing brain maturation in our young rats, dissecting changes related to brain maturation, CRS, and LI-rTMS is difficult. For example, an increase in FA has consistently been reported in patients with depression following repeated high-frequency rTMS (71,72) and electroconvulsive therapy (73,74). In contrast, in this study, FA increased over time in all three CRS groups, suggesting that there was no effect of LI-rTMS on FA. However, we cannot rule out that changes in FA due to LI-rTMS were masked by ongoing maturation.

Nonetheless, some measures were specific to LI-rTMS, and these were consistent with an increase in myelination. Myelination has been positively correlated to FC in previous animal studies combining dMRI and immunohistochemistry (75) and in human dMRI studies of demyelinating diseases (76,77). We observed a greater increase in FC in the active group, consistent with their higher level of MBP in the corpus callosum compared with sham and depression control groups. The combination of an increase in FC and myelination in the corpus callosum (78) reflects normal cerebral development in rats, and these changes typically continue well into adulthood (3–6 mo) but were impaired in sham and depression control animals. It is well established that exposure to early life stress alters WM development in humans, nonhuman primates, and rodents (79). In addition, abnormal myelination has been reported in human patients with depression and animal models of depression and anxiety-like behaviors (15,80). Therefore, our results suggest that LI-rTMS may rescue brain maturation-related and/or CRS-related changes, potentially via increased survival of oligodendrocytes and/or increased myelin production (81).

Because neuronal activity is a major regulator of oligodendrocyte biology during development and in adulthood (81,82), brain stimulation is a compelling therapeutic approach to promote myelin repair. Low-intensity magnetic stimulation as used in this study has been shown to increase survival of newly generated oligodendrocytes in mice (81), which may underpin the increased myelination observed in our experiments. Low-intensity magnetic stimulation does not trigger action potentials (83,84) but has been shown to increase excitability of pyramidal neurons in cortical slices (85) and alter conduction velocity of axons in the corpus callosum (86). These changes to intrinsic neuronal properties may alter the probability of neuronal firing, leading to the increased myelination described in both studies. It is possible that higher intensities of rTMS, such as those used in clinical settings, might have the same outcomes; direct electrical stimulation to the corticospinal tract at suprathreshold intensities results in proliferation and differentiation of oligodendrocyte progenitor cells (87). Although both stimulation protocols would ultimately increase myelination, it is interesting to note that they likely do so via different mechanisms.

Study Limitations and Future Directions

Our study has two main limitations. First, dMRI cannot directly measure microstructural changes, which need to be confirmed using invasive methods in animal studies. For example, retrograde tract-tracing data together with immunohistochemistry of gliosis status can further verify dMRI changes. Second, older adult rats that have completed cerebral development (6 mo or older) can be used to exclude brain maturation–related changes seen in this study. Nonetheless, combining the use of DKI and conventional DTI along with fixel-based WM tractography improved the detection of changes induced by CRS and LI-rTMS and provided more directionally specific and complementary information compared with using these approaches individually. These findings suggest that multiple diffusion and kurtosis parameters should be used in conjunction with AFD and track-weighted imaging measures to assist in further advancing our understanding of depression disease progression and rTMS treatment.

Conclusions

In conclusion, this study found evidence of delayed brain maturation–related changes in restrained animals, but these were partly rescued by LI-rTMS. By integrating dMRI and immunohistochemistry, our results raise the possibility that LI-rTMS and potentially rTMS may exert therapeutic effects by rescuing abnormal myelination, in addition to their well-characterized effects on neuronal plasticity (50), providing new insight into their mechanism of action and potential therapeutic applications.

ACKNOWLEDGMENTS AND DISCLOSURES

This research was funded by the University of Western Australia, a Forrest Research Foundation Scholarship (to BJS), an International Postgraduate Research Scholarship (to BJS), a University Postgraduate Award (to BJS), an Australian National Imaging Facility Fellow (a facility funded by the University, State, and Commonwealth Governments) (to KWF), a University Postgraduate Award at the University of Western Australia (to LAH), the Commonwealth Government's Australian Government Research Training Program Fees Offset (to LAH), a Fellowship from MSWA (to JR), and the Perron Institute for Neurological and Translational Science (to JR).

We thank Dr. Sarah Etherington, Ms. Marissa Penrose-Menz, Ms. Kerry Leggett, Ms. Elizabeth Jaeschke-Angi, Ms. Leah Mackie, Ms. Kaylene Schutz, Ms. Yasmin Arena-Foster, Ms. Michelle Carey, Ms. Katherine Fisher, Mr. Rex Edwards, Mr. Samuel Bolland, Ms. Elena Faessler, Mr. Erik Stefan, Ms. Tess Wheeler, Ms. Samantha Musgrave, Mr. David Gerard, Ms. Yashvi Bhatt, and Mr. Parth Patel for their assistance with the experiments. We also thank the team at University of Western Australia M Block Animal Care Services for their assistance with animal care and transport. We also acknowledge the facilities and scientific and technical assistance of the National Imaging Facility, a National Collaborative Research Infrastructure Strategy capability, at the Centre for Microscopy Characterisation and Analysis, the University of Western Australia.

The authors report no biomedical financial interests or potential conflicts of interest.

ARTICLE INFORMATION

From Experimental and Regenerative Neurosciences (BJS, AF, LAH, JR), School of the Biological Sciences, The University of Western Australia; Centre for Microscopy, Characterisation & Analysis (BJS, KWF, ACJ), Research Infrastructure Centres, The University of Western Australia; School of Biomedical Sciences (KWF), The University of Western Australia; and School of Human Sciences (YW), The University of Western Australia, Crawley; Brain Plasticity Group (BJS, AF, LAH, JR), Perron Institute for Neurological and Translational Science, Nedlands; and the School of Veterinary and Life Sciences (AF), Murdoch University, Murdoch, Western Australia, Australia.

Address correspondence to Jennifer Rodger, Ph.D., at jennifer.rodger@uwa.edu.au.

Received May 3, 2021; revised Jul 27, 2021; accepted Aug 16, 2021.

Supplementary material cited in this article is available online at https://doi.org/10.1016/j.bpsgos.2021.08.006.

REFERENCES

1. Ridding MC, Ziemann U (2010): Determinants of the induction of cortical plasticity by non-invasive brain stimulation in healthy subjects. J Physiol 588:2291–2304.
2. O'Reardon JP, Solvason HB, Janicak PG, Sampson S, Isenberg KE, Nahas Z, *et al.* (2007): Efficacy and safety of transcranial magnetic stimulation in the acute treatment of major depression: A multisite randomized controlled trial. Biol Psychiatry 62:1208–1216.
3. Krishnan V, Nestler EJ (2011): Animal models of depression: Molecular perspectives. Curr Top Behav Neurosci 7:121–147.
4. Suvrathan A, Tomar A, Chattarji S (2010): Effects of chronic and acute stress on rat behaviour in the forced-swim test. Stress 13:533–540.
5. Seewoo BJ, Hennessy LA, Feindel KW, Etherington SJ, Croarkin PE, Rodger J (2020): Validation of chronic restraint stress model in young adult rats for the study of depression using longitudinal multimodal MR imaging. eNeuro 7: ENEURO.0113-20.2020.
6. Hunter RG, Seligsohn M, Rubin TG, Griffiths BB, Ozdemir Y, Pfaff DW, *et al.* (2016): Stress and corticosteroids regulate rat hippocampal mitochondrial DNA gene expression via the glucocorticoid receptor. Proc Natl Acad Sci U S A 113:9099–9104.
7. Ampuero E, Luarte A, Santibañez M, Varas-Godoy M, Toledo J, Diaz-Veliz G, *et al.* (2015): Two chronic stress models based on movement restriction in rats respond selectively to antidepressant drugs: Aldolase C as a potential biomarker. Int J Neuropsychopharmacol 18:pyv038.
8. Henckens MJAG, van der Marel K, van der Toorn A, Pillai AG, Fernández G, Dijkhuizen RM, Joëls M (2015): Stress-induced alterations in large-scale functional networks of the rodent brain. NeuroImage 105:312–322.
9. Alemu JL, Elberling F, Azam B, Pakkenberg B, Olesen MV (2019): Electroconvulsive treatment prevents chronic restraint stress-induced atrophy of the hippocampal formation-A stereological study. Brain Behav 9:e01195.
10. Vyas A, Mitra R, Shankaranarayana Rao BS, Chattarji S (2002): Chronic stress induces contrasting patterns of dendritic remodeling in hippocampal and amygdaloid neurons. J Neurosci 22:6810–6818.
11. Ota M, Noda T, Sato N, Hattori K, Hori H, Sasayama D, *et al.* (2015): White matter abnormalities in major depressive disorder with melancholic and atypical features: A diffusion tensor imaging study. Psychiatry Clin Neurosci 69:360–368.
12. Kamiya K, Okada N, Sawada K, Watanabe Y, Irie R, Hanaoka S, *et al.* (2018): Diffusional kurtosis imaging and white matter microstructure modeling in a clinical study of major depressive disorder. NMR Biomed 31:e3938.
13. Hemanth Kumar BS, Mishra SK, Trivedi R, Singh S, Rana P, Khushu S (2014): Demyelinating evidences in CMS rat model of depression: A DTI study at 7T. Neuroscience 275:12–21.
14. Zalsman G, Weller A, Shbiro L, Barzilay R, Gutman A, Weizman A, *et al.* (2017): Fibre tract analysis using diffusion tensor imaging reveals aberrant connectivity in a rat model of depression. World J Biol Psychiatry 18:615–623.
15. Sacchet MD, Gotlib IH (2017): Myelination of the brain in major depressive disorder: An in vivo quantitative magnetic resonance imaging study. Sci Rep 7:2200.
16. Lehmann ML, Weigel TK, Elkahloun AG, Herkenham M (2017): Chronic social defeat reduces myelination in the mouse medial prefrontal cortex. Sci Rep 7:46548.
17. Guglielmetti C, Veraart J, Roelant E, Mai Z, Daans J, Van Audekerke J, *et al.* (2016): Diffusion kurtosis imaging probes cortical alterations and white matter pathology following cuprizone induced demyelination and spontaneous remyelination. Neuroimage 125:363–377.
18. Falangola MF, Guilfoyle DN, Tabesh A, Hui ES, Nie X, Jensen JH, *et al.* (2014): Histological correlation of diffusional kurtosis and white matter modeling metrics in cuprizone-induced corpus callosum demyelination. NMR Biomed 27:948–957.
19. Seewoo BJ, Feindel KW, Etherington SJ, Rodger J (2019): Frequency-specific effects of low-intensity rTMS can persist for up to 2 weeks post-stimulation: A longitudinal rs-fMRI/MRS study in rats. Brain Stimul 12:1526–1536.
20. Rodger J, Mo C, Wilks T, Dunlop SA, Sherrard RM (2012): Transcranial pulsed magnetic field stimulation facilitates reorganization of abnormal neural circuits and corrects behavioral deficits without disrupting normal connectivity. FASEB J 26:1593–1606.
21. Makowiecki K, Harvey AR, Sherrard RM, Rodger J (2014): Low-intensity repetitive transcranial magnetic stimulation improves abnormal visual cortical circuit topography and upregulates BDNF in mice. J Neurosci 34:10780–10792.
22. Seewoo BJ, Feindel KW, Etherington SJ, Rodger J (2018): Resting-state fMRI study of brain activation using low-intensity repetitive transcranial magnetic stimulation in rats. Sci Rep 8:6706.
23. Seewoo B, Feindel K, Etherington S, Hennessy L, Croarkin P, Rodger J (2019): M85. Validation of the chronic restraint stress model of depression in rats and investigation of standard vs accelerated rTMS treatment. Neuropsychopharmacology 44:122–123.
24. Tournier JD, Smith R, Raffelt D, Tabbara R, Dhollander T, Pietsch M, *et al.* (2019): MRtrix3: A fast, flexible and open software framework for medical image processing and visualisation. Neuroimage 202:116137.
25. Veraart J, Novikov DS, Christiaens D, Ades-Aron B, Sijbers J, Fieremans E (2016): Denoising of diffusion MRI using random matrix theory. Neuroimage 142:394–406.
26. Cordero-Grande L, Christiaens D, Hutter J, Price AN, Hajnal JV (2019): Complex diffusion-weighted image estimation via matrix recovery under general noise models. Neuroimage 200:391–404.
27. Veraart J, Fieremans E, Novikov DS (2016): Diffusion MRI noise mapping using random matrix theory. Magn Reson Med 76:1582–1593.
28. Kellner E, Dhital B, Kiselev VG, Reisert M (2016): Gibbs-ringing artifact removal based on local subvoxel-shifts. Magn Reson Med 76:1574–1581.
29. Tustison NJ, Avants BB, Cook PA, Zheng Y, Egan A, Yushkevich PA, Gee JC (2010): N4ITK: Improved N3 bias correction. IEEE Trans Med Imaging 29:1310–1320.
30. C Wood T (2018): QUIT: QUantitative imaging tools. J Open Source Softw 3:656.
31. Smith SM, Jenkinson M, Johansen-Berg H, Rueckert D, Nichols TE, Mackay CE, *et al.* (2006): Tract-based spatial statistics: Voxelwise analysis of multi-subject diffusion data. Neuroimage 31:1487–1505.
32. Jenkinson M, Beckmann CF, Behrens TE, Woolrich MW, Smith SM (2012). FSL. Neuroimage 62:782–790.
33. Tabesh A, Jensen JH, Ardekani BA, Helpern JA (2011): Estimation of tensors and tensor-derived measures in diffusional kurtosis imaging. Magn Reson Med 65:823–836.
34. Zhang H, Avants BB, Yushkevich PA, Woo JH, Wang S, McCluskey LF, *et al.* (2007): High-dimensional spatial normalization of diffusion tensor images improves the detection of white matter differences: An example study using amyotrophic lateral sclerosis. IEEE Trans Med Imaging 26:1585–1597.
35. Zhang H, Yushkevich PA, Alexander DC, Gee JC (2006): Deformable registration of diffusion tensor MR images with explicit orientation optimization. Med Image Anal 10:764–785.
36. Harris NG, Verley DR, Gutman BA, Sutton RL (2016): Bi-directional changes in fractional anisotropy after experiment TBI: Disorganization and reorganization? Neuroimage 133:129–143.
37. Raffelt DA, Smith RE, Ridgway GR, Tournier JD, Vaughan DN, Rose S, *et al.* (2015): Connectivity-based fixel enhancement: Whole-brain statistical analysis of diffusion MRI measures in the presence of crossing fibres. Neuroimage 117:40–55.
38. Raffelt D, Tournier JD, Rose S, Ridgway GR, Henderson R, Crozier S, *et al.* (2012): Apparent Fibre Density: A novel measure for the analysis

of diffusion-weighted magnetic resonance images. Neuroimage 59:3976–3994.
39. Wright DK, Johnston LA, Kershaw J, Ordidge R, O'Brien TJ, Shultz SR (2017): Changes in apparent fiber density and track-weighted imaging metrics in white matter following experimental traumatic brain injury. J Neurotrauma 34:2109–2118.
40. Raffelt DA, Tournier JD, Smith RE, Vaughan DN, Jackson G, Ridgway GR, Connelly A (2017): Investigating white matter fibre density and morphology using fixel-based analysis. Neuroimage 144:58–73.
41. Tournier JD, Calamante F, Connelly A (2010): Improved probabilistic streamlines tractography by 2nd order integration over fibre orientation distributions. In: Proceedings of the International Society for Magnetic Resonance in Medicine. New Jersey: John Wiley & Sons, Inc.
42. Pannek K, Mathias JL, Bigler ED, Brown G, Taylor JD, Rose SE (2011): The average pathlength map: A diffusion MRI tractography-derived index for studying brain pathology. NeuroImage 55:133–141.
43. Smith SM, Nichols TE (2009): Threshold-free cluster enhancement: Addressing problems of smoothing, threshold dependence and localisation in cluster inference. NeuroImage 44:83–98.
44. Nichols TE, Holmes AP (2002): Nonparametric permutation tests for functional neuroimaging: A primer with examples. Hum Brain Mapp 15:1–25.
45. Winkler AM, Ridgway GR, Webster MA, Smith SM, Nichols TE (2014): Permutation inference for the general linear model. Neuroimage 92:381–397.
46. Yushkevich PA, Piven J, Hazlett HC, Smith RG, Ho S, Gee JC, Gerig G (2006): User-guided 3D active contour segmentation of anatomical structures: Significantly improved efficiency and reliability. Neuroimage 31:1116–1128.
47. Paxinos G, Watson C, Calabrese E, Badea A, Johnson GA (2015): MRI/DTI Atlas of the Rat Brain. San Diego: Academic Press.
48. Schindelin J, Arganda-Carreras I, Frise E, Kaynig V, Longair M, Pietzsch T, *et al.* (2012): Fiji: An open-source platform for biological-image analysis. Nat Methods 9:676–682.
49. Wu EX, Cheung MM (2010): MR diffusion kurtosis imaging for neural tissue characterization. NMR Biomed 23:836–848.
50. Tang A, Thickbroom G, Rodger J (2017): Repetitive transcranial magnetic stimulation of the brain: Mechanisms from animal and experimental models. Neuroscientist 23:82–94.
51. Seewoo BJ, Etherington SJ, Feindel KW, Rodger J (2018): Combined rTMS/fMRI studies: An overlooked resource in animal models. Front Neurosci 12:180.
52. Arnone D, Mumuni AN, Jauhar S, Condon B, Cavanagh J (2015): Indirect evidence of selective glial involvement in glutamate-based mechanisms of mood regulation in depression: Meta-analysis of absolute prefrontal neuro-metabolic concentrations. Eur Neuropsychopharmacol 25:1109–1117.
53. Pell GS, Roth Y, Zangen A (2011): Modulation of cortical excitability induced by repetitive transcranial magnetic stimulation: Influence of timing and geometrical parameters and underlying mechanisms. Prog Neurobiol 93:59–98.
54. Niehaus L, Hoffmann KT, Grosse P, Röricht S, Meyer BU (2000): MRI study of human brain exposed to high-dose repetitive magnetic stimulation of visual cortex. Neurology 54:256–258.
55. Mottaghy FM, Gangitano M, Horkan C, Chen Y, Pascual-Leone A, Schlaug G (2003): Repetitive TMS temporarily alters brain diffusion. Neurology 60:1539–1541.
56. Abe M, Fukuyama H, Mima T (2014): Water diffusion reveals networks that modulate multiregional morphological plasticity after repetitive brain stimulation. Proc Natl Acad Sci U S A 111:4608–4613.
57. Müller-Dahlhaus F, Vlachos A (2013): Unraveling the cellular and molecular mechanisms of repetitive magnetic stimulation. Front Mol Neurosci 6:50.
58. Mengler L, Khmelinskii A, Diedenhofen M, Po C, Staring M, Lelieveldt BPF, Hoehn M (2014): Brain maturation of the adolescent rat cortex and striatum: Changes in volume and myelination. NeuroImage 84:35–44.
59. van Velzen LS, Kelly S, Isaev D, Aleman A, Aftanas LI, Bauer J, *et al.* (2020): White matter disturbances in major depressive disorder: A coordinated analysis across 20 international cohorts in the ENIGMA MDD working group. Mol Psychiatry 25:1511–1525.
60. Tymofiyeva O, Connolly CG, Ho TC, Sacchet MD, Henje Blom E, LeWinn KZ, *et al.* (2017): DTI-based connectome analysis of adolescents with major depressive disorder reveals hypoconnectivity of the right caudate. J Affect Disord 207:18–25.
61. Chen G, Hu X, Li L, Huang X, Lui S, Kuang W, *et al.* (2016): Disorganization of white matter architecture in major depressive disorder: A meta-analysis of diffusion tensor imaging with tract-based spatial statistics. Sci Rep 6:21825.
62. McIntosh AL, Gormley S, Tozzi L, Frodl T, Harkin A (2017): Recent advances in translational magnetic resonance imaging in animal models of stress and depression. Front Cell Neurosci 11:150.
63. Nagy SA, Vranesics A, Varga Z, Csabai D, Bruszt N, Bali ZK, *et al.* (2020): Stress-induced microstructural alterations correlate with the cognitive performance of rats: A Longitudinal in vivo diffusion tensor imaging study. Front Neurosci 14:474.
64. Wang T, Huang X, Huang P, Li D, Lv F, Zhang Y, *et al.* (2013): Early-stage psychotherapy produces elevated frontal white matter integrity in adult major depressive disorder. PLoS One 8:e63081.
65. Blood AJ, Iosifescu DV, Makris N, Perlis RH, Kennedy DN, Dougherty DD, *et al.* (2010): Microstructural abnormalities in subcortical reward circuitry of subjects with major depressive disorder. PLoS One 5:e13945.
66. Zhao L, Wang Y, Jia Y, Zhong S, Sun Y, Zhou Z, *et al.* (2016): Cerebellar microstructural abnormalities in bipolar depression and unipolar depression: A diffusion kurtosis and perfusion imaging study. J Affect Disord 195:21–31.
67. Khan AR, Chuhutin A, Wiborg O, Kroenke CD, Nyengaard JR, Hansen B, Jespersen SN (2016): Biophysical modeling of high field diffusion MRI demonstrates micro-structural aberration in chronic mild stress rat brain. NeuroImage 142:421–430.
68. Coloigner J, Batail JM, Commowick O, Corouge I, Robert G, Barillot C, Drapier D (2019): White matter abnormalities in depression: A categorical and phenotypic diffusion MRI study. Neuroimage Clin 22:101710.
69. Shizukuishi T, Abe O, Aoki S (2013): Diffusion tensor imaging analysis for psychiatric disorders. Magn Reson Med Sci 12:153–159.
70. Magalhães R, Bourgin J, Boumezbeur F, Marques P, Bottlaender M, Poupon C, *et al.* (2017): White matter changes in microstructure associated with a maladaptive response to stress in rats. Transl Psychiatry 7:e1009.
71. Kozel FA, Johnson KA, Nahas Z, Nakonezny PA, Morgan PS, Anderson BS, *et al.* (2011): Fractional anisotropy changes after several weeks of daily left high-frequency repetitive transcranial magnetic stimulation of the prefrontal cortex to treat major depression. J ECT 27:5–10.
72. Peng H, Zheng H, Li L, Liu J, Zhang Y, Shan B, *et al.* (2012): High-frequency rTMS treatment increases white matter FA in the left middle frontal gyrus in young patients with treatment-resistant depression. J Affect Disord 136:249–257.
73. Lyden H, Espinoza RT, Pirnia T, Clark K, Joshi SH, Leaver AM, *et al.* (2014): Electroconvulsive therapy mediates neuroplasticity of white matter microstructure in major depression. Transl Psychiatry 4:e380.
74. Nobuhara K, Okugawa G, Minami T, Takase K, Yoshida T, Yagyu T, *et al.* (2004): Effects of electroconvulsive therapy on frontal white matter in late-life depression: A diffusion tensor imaging study. Neuropsychobiology 50:48–53.
75. Malhotra A, Sepehrizadeh T, Dhollander T, Wright D, Castillo-Melendez M, Sutherland AE, *et al.* (2019): Advanced MRI analysis to detect white matter brain injury in growth restricted newborn lambs. Neuroimage Clin 24:101991.
76. Gajamange S, Raffelt D, Dhollander T, Lui E, van der Walt A, Kilpatrick T, *et al.* (2018): Fibre-specific white matter changes in multiple sclerosis patients with optic neuritis. Neuroimage Clin 17:60–68.

77. Storelli L, Pagani E, Preziosa P, Filippi M, Rocca MA (2021): Measurement of white matter fiber-bundle cross-section in multiple sclerosis using diffusion-weighted imaging. Mult Scler 27:818–826.
78. Nuñez JL, Nelson J, Pych JC, Kim JHY, Juraska JM (2000): Myelination in the splenium of the corpus callosum in adult male and female rats. Brain Res Dev Brain Res 120:87–90.
79. Islam R, Kaffman A (2021): White-matter repair as a novel therapeutic target for early adversity. Front Neurosci 15:657693.
80. Liu J, Dietz K, DeLoyht JM, Pedre X, Kelkar D, Kaur J, *et al.* (2012): Impaired adult myelination in the prefrontal cortex of socially isolated mice. Nat Neurosci 15:1621–1623.
81. Cullen CL, Senesi M, Tang AD, Clutterbuck MT, Auderset L, O'Rourke ME, *et al.* (2019): Low-intensity transcranial magnetic stimulation promotes the survival and maturation of newborn oligodendrocytes in the adult mouse brain. Glia 67:1462–1477.
82. Barres BA, Raff MC (1993): Proliferation of oligodendrocyte precursor cells depends on electrical activity in axons. Nature 361:258–260.
83. Grehl S, Viola HM, Fuller-Carter PI, Carter KW, Dunlop SA, Hool LC, *et al.* (2015): Cellular and molecular changes to cortical neurons following low intensity repetitive magnetic stimulation at different frequencies. Brain Stimul 8:114–123.
84. Tang AD, Lowe AS, Garrett AR, Woodward R, Bennett W, Canty AJ, *et al.* (2016): Construction and evaluation of rodent-specific rTMS coils. Front Neural Circuits 10:47.
85. Tang AD, Hong I, Boddington LJ, Garrett AR, Etherington S, Reynolds JNJ, Rodger J (2016): Low-intensity repetitive magnetic stimulation lowers action potential threshold and increases spike firing in layer 5 pyramidal neurons in vitro. Neuroscience 335:64–71.
86. Cullen CL, Pepper RE, Clutterbuck MT, Pitman KA, Oorschot V, Auderset L, *et al.* (2021): Periaxonal and nodal plasticities modulate action potential conduction in the adult mouse brain. Cell Rep 34:108641.
87. Li Q, Brus-Ramer M, Martin JH, McDonald JW (2010): Electrical stimulation of the medullary pyramid promotes proliferation and differentiation of oligodendrocyte progenitor cells in the corticospinal tract of the adult rat. Neurosci Lett 479:128–133.